Sustainable ammonia synthesis from nitrogen wet with sea water vapor by single-step plasma catalysis

Hoang M. Nguyen[†], Fnu Gorky[†], Shelby Guthrie[†], Maria L. Carreon[*,†]

[†]Mechanical Engineering Department, University of Massachusetts Lowell, One University Avenue, Lowell, Massachusetts 01854-5043, USA.

Corresponding Author

E-mail address: Maria_Carreon@uml.edu (Maria L. Carreon).

Abstract. Ammonia synthesis at ambient conditions employing intermittent distributed green sources of energy and feedstocks is globally sought to replace the centralized Haber-Bosch (H-B) process operating at high temperature and pressure. We report herein for the first time an effective and sustainable ammonia synthesis pathway from N_2 wet with seawater vapor over spherical SiO_2 and M/SiO_2 (M: Ag, Cu, and Co) catalysts driven by non-thermal plasma (NTP). Experimental results indicate that the presence of a catalyst is required for ammonia production from seawater vapor and N_2. The Co/SiO_2 catalyst delivered the highest ammonia synthesis rate (r_{NH_3}) of 3.7 mmol.g_{cat}^{-1}.h^{-1} and energy yield of 3.2 $g_{NH_3}.kW^{-1}.h^{-1}$ at a relatively low input power of 2 W. The extraction of H atoms from H_2O molecules plays an important role in the ammonia synthesis from seawater vapor. This work unfolds a novel platform for the subsequent optimization of sustainable ammonia production from endless resources such as seawater and N_2 through catalytic non-thermal plasma potentially powered by renewable sources.

Keywords: Non-thermal plasma, plasma catalyst, sustainable ammonia synthesis, silica catalyst, seawater vapor, ammonia.

1. Introduction

Ammonia plays a crucial role in the agricultural industry as a primary element for fertilizer production and it is also a foundational feedstock for pharmaceuticals, dyes, and chemical synthesis [1]. Ammonia has also emerged as an energy carrier and transportation fuel. Ammonia consists of 17.6 wt % of hydrogen, and thereby, it can be used as an indirect hydrogen storage compound [2]. Moreover, ammonia's energy density is approximately 4.32 $kWh.L^{-1}$, showing a capacity equivalently to methanol and almost double than that of liquid hydrogen [3]. Recently, automobiles operating on pure ammonia and gasoline-ammonia fuel modifications are being hypothesized and near to be prototyped [4, 5]. An important advantage of using pure ammonia is the resulting diminished reliance on fossil fuels by changing to a "sustainable fuel source" that can be manufactured synthetically [6]. Soon synthetic low-carbon fuels will be needed as a response to the current environmental emergency, and ammonia is among such synthetic fuels.

Currently, the most commonly-used technology for ammonia production is the Haber-Bosch (H-B) process, which requires high energy input and emits greenhouse gas largely to achieve its harsh operating conditions i.e., high reaction temperature (400 – 500 ^{o}C) and high pressure (150 – 300 atm) [7-9]. Such large intrinsic carbon footprint technology for ammonia synthesis secures a long-standing need for the development of alternative processes that operate under milder conditions such as low temperature, atmospheric pressure, and even more preferably, with zero carbon emissions. A possible solution to fulfill this goal is the use of regionalized synthesis processes powered by renewable energy resources, which can even exploit benefits from local resources, particularly in remote areas. Another challenge of the current ammonia synthesis is the use of "expensive" feed i.e., hydrogen. While hydrogen is considered a "green fuel" to replace fossil fuels, the use of such a valuable chemical as a feedstock for ammonia production is uneconomical. More importantly, the energy cost of hydrogen production originates from the energy-intensive methane reforming process operated

at high temperature i.e., 800-1000 ^{o}C [10]. The produced hydrogen also needs to be stored and transported, posing safety concerns, and high downstream costs [11]. Therefore, alternative sustainable pathways for ammonia production will draw important attention from researchers and industries. The use of H_2O as a hydrogen source in the synthesis of ammonia is one of the most promising approaches when employing non-thermal plasma (NTP) in a sustainable and economical way. Nonetheless, most of the studies on the production of ammonia from N_2 and H_2O have been focused on photochemical, electrochemical routes, or hybrid plasma-activated electrolysis [12-17]. These processes are reported to operate under mild conditions. Despite the N_2 reduction determining the final ammonia synthesis yield there is an important competition with the hydrogen evolution reactions from such electrochemical-based processes, which are challenging to control [18, 19]. In addition, the electron energy transferred to N_2 molecules in these two processes is insufficient to dissociate its high bonding energy (N≡N, 9.8 eV), and thereby, the resultant ammonia production rate is relatively low [20, 21]. Electrochemical process for hydrogen production from water splitting is currently far from industrial application because of technical problems associated with electrode stability and electrolyser design/scale-up [18]. Hybrid plasma-electrochemical systems reducing N_2 with water show high potential for scale-up with high ammonia yield [22]. Nevertheless, such systems are complicated and require high capital investment to obtain a desirable high ammonia synthesis yield. In comparison to the mentioned processes, non-thermal plasma with highly energetic electrons, and in the presence of a catalyst i.e., plasma catalytic system can result in the activation of the highly stable N_2 molecules into more reactive, vibrationally or electronically excited states, enabling thermodynamically unfavourable reactions to occur at ambient conditions on selected catalytic surfaces [23, 24]. Moreover, dielectric barrier discharge (DBD) plasma reactors can be straightforward turned on/off suitable for storing intermittent energy [25]. This added to their conceptualization as modular small-scale systems for ammonia synthesis results in simple lightweight units compared to high pressure thermal reactors, which comprise added complex

insulation/cooling systems [26]. Indeed, our group has studied ammonia synthesis over NTP catalytic processes over the past years [27-32]. The achieved fundamental understanding on the effects of different catalysts, plasma-catalyst synergisms, and energy efficiency on ammonia synthesis allow us to primarily estimate the great potential of ammonia synthesis from N_2 and "green" H_2 sources, which is an important step to achieve zero-carbon ammonia synthesis. Zhang and co-workers have pioneer the substitution of H_2 by water [33, 34] for plasma-assisted ammonia synthesis over a notable supported Ru catalyst and obtain an ammonia synthesis rate of around 2.7 $mmol.g_{cat}^{-1}.h^{-1}$. However, much needs to be done in this respect, especially when exploring less costing materials that can show enhanced behaviour in plasma environments. The potential implementation of non-thermal plasma technology will not be feasible until there is a competitive plasma catalytic system in terms of material selection and reactor design. New approaches are needed for intelligent design of catalytic materials and the chosen materials must pair well with efficient plasma reactors. As a choice of catalytic materials, solid oxides are robust, efficient and low-cost materials for catalytic applications. Besides their low cost, they offer textural, compositional, and morphological properties that can be tailored for diverse targeted catalytic reactions [35]. Specially, silica is an appealing material for plasma catalytic ammonia synthesis due to: (i) its low electrical resistivity that can lead to more stable and uniform plasma discharges; [36] (ii) readiness to dissolve hydrogen;[37] (iii) weak bonding with nitrogen;[38] (iv) high thermal and chemical stability in the presence of water, which is the source of hydrogen in this work. Our catalyst selection is supported by our group's previous experience on the rational design of catalysts for ammonia synthesis [27, 30, 39]. Moreover, it has been indicated that silica-based catalysts promote the decomposition of N_2O [40, 41], which is an unwanted by-product during ammonia production from water and N_2 [33].

Given its wide availability, seawater is the most suitable and sustainable replacement for hydrogen in ammonia synthesis powered by NTP. The previously described challenges and

opportunities have motivated us to substitute of H_2 by seawater during the synthesis of ammonia powered by a dielectric-barrier discharge (DBD) non-thermal plasma. To benchmark and compare the ammonia synthesis rate obtained from N_2 wet with seawater vapor a feed mixture of H_2 and N_2 was also employed for NTP-assisted ammonia synthesis. We have found the excellent ammonia synthesis rate of 3.7 $mmol.g_{cat}^{-1}.h^{-1}$ and the energy yield of 3.2 $g_{NH_3}.kW^{-1}.h^{-1}$ at a low plasma input power of 2 W over the Co/SiO_2 catalyst. Plausible insights of ammonia formation pathways from N_2 and seawater vapor are elucidated. This work demonstrates the initial steps towards a straightforward single-step process to dissociate both water vapor and N_2 molecules driven by atmospheric catalytic NTP to produce ammonia sustainably and economically.

2. Experimental section

2.1. Chemicals and materials. Polyethylene-block-poly(ethylene glycol) (Sigma Aldrich, average Mn ~920), deionized water, tetraethyl orthosilicate (TEOS, Sigma Aldrich, 99.9%), toluene (Sigma Aldrich, 99.5%), silver nitrate (Sigma Aldrich, 99.5%), cobalt nitrate (Sigma Aldrich, 99.5%), copper nitrate (Sigma Aldrich, 99.5%), ammonium hydroxide solution (NH_4OH, 32 %, Sigma Aldrich), polystyrene microspheres (PS, Sigma Aldrich), and ethanol (70%, Sigma Aldrich). Seawater was collected from Rockport, Massachusetts, USA and used directly without further processing (**Fig. S1**).

2.2. Catalyst preparation.

2.2.1. Synthesis of silica spheres. A first solution was prepared by mixing 100 g of ethanol, 40 mL of NH_4OH and 6 g of Polyethylene-block-poly (ethylene glycol). A second solution consisting of 40 g toluene, 4 g PS beads, and 20 g deionized water was prepared. These two solutions were stirred separately for 30 mins before mixing them and stirring for 2 hrs. Then, 26 g of TEOS was added to the solution and kept stirring for 10 hours at 90 ^oC and 360 rpm. The obtained white gel was calcined at 650 ^oC for 4 h with a heating rate of 1 $^oC \cdot min^{-1}$ in air.

2.2.2. Synthesis of silica supported metal catalysts. The M/SiO_2 (M: Ag, Cu, and Co) catalysts were prepared by incipient wetness impregnation method using metallic nitrates as precursors. The samples were calcined at 500 °C for 4 hrs with a heating rate of 1 $^oC.min^{-1}$. The nominal metal fraction was calculated by the ratio of metal mass (g) from its respective salt per the SiO_2 mass. This step aims to secure the metal content of 3 wt.% in the prepared catalysts.

2.3. Catalyst characterization. Powder X-ray diffraction (XRD) patterns were collected on a 3rd generation Empyrean, Malvern Panalytical (Cobalt Source), operated at 45 mA and 40 kV. The diffraction peaks were collected over a range of 2θ of 10-70° with a scanning step size of 0.01° and a time of 2 s. Raman Spectroscopy was employed for detailed molecular interaction information. The experiments were conducted under room temperature in a Micro-Raman Spectrometer and Raman microscope (Foster and Freeman) at 638 nm with accessible laser output power between 4.5-5 mW (maximum power output of 9 mW). All catalysts were tested at multiple points over microscopic slides in pentaplicates and further averaged. For the presented data, the instrument was calibrated before each sample was loaded, the catalyst was carefully spread on a polystyrene microscopic slide (25*75 mm). The average scanning time (15-18 seconds/scan) was automated via FORAMX3 software. Counts were increased to 10 for refining the Raman shifts (cm^{-1}). Raman bands are often influenced by strain, particle distribution, vibration bands of amorphous silica and presence of surface species. For the presented data, the wavelength of 638 nm was selected for sharp visualization of peaks and lower signal-to-noise ratio at higher wavenumber (cm^{-1}). The morphologies of the catalysts were characterized by using scanning electron microscopy (SEM) JEOL JSM-7401F, with an acceleration voltage of 5 kV. The metallic concentration was verified by using ICP-OES equipment (NexION™ 350D-Optima 8300, PerkinElmer). Whereby, 1 mg of each catalyst sample was digested in a 5 % HNO_3 solution prior to analysis. The measurement was performed at room temperature and in triplicates.

2.4. Plasma-driven ammonia synthesis reaction. The experimental setup for ammonia synthesis reaction is shown in **Fig. S2**. Different input N_2 flowrates were employed i.e., 3.1, 6.2, 12.5, and 25.0 sccm when using water vapor as hydrogen source. Similar input N_2 flowrate range was employed in ammonia production from N_2/H_2 mixtures with the input H_2 flowrate fixed at 12.5 sccm. Seawater was contained in a 500 mL DURAN© washing flask container. The relative humidity (RH%) of inlet N_2 gas was 100 % at 20 ^oC and atmospheric pressure.[33] The effluent headline of the input N_2 gas pipeline was dipped to the bottom of the seawater container to secure maximum contact with the seawater. This step was performed at room temperature. The humid gas was passed through a packed-bed DBD reactor made of quartz tube (I.D. of 4 mm and O.D. of 6.40 mm) with coaxial tungsten rod electrode (2.4 mm diameter) and copper mesh grounding. The inner electrode was made of tungsten, and it was placed at the center of the quartz tube. For each experiment, 100 mg of catalyst in fine powder form was packed in the center of the quartz tube reactor. Quartz frits were placed at the input and output of the reactor to prevent any possible catalyst displacement under the gas flow. To ensure that all ammonia was captured, the gas was bubbled in deionized water. The reactor exhaust was connected directly to an Agilent 8860A GC operating with a HP-PLOT U column (30 m × 0.32 mm × 10 μm) with hydrogen gas as a carrier. The light emitted from the discharge was led through an optical system. The measurements were recorded using a dual channel UV−vis−NIR spectrophotometer (Avantes Inc., USB2000 Series) in a scope mode. The spectral range was from 200 to 1100 nm, using a line grating of 600 lines/mm and a resolution of 0.4 nm. A bifurcated fiber optic cable of 400 μm was employed. Acceptance angle and location: emission spectra of the glow region were measured at the center of the tube since the catalyst was packed in the center of the tube. The fiber optical cable was positioned at the center of the reactor, and the distance between the reactor and fiber optical cable was 7 cm, consistent throughout the collection. The UV−vis−NIR spectrophotometer focuses the exit light under 90°. Standard optical fibers have a numerical aperture of 0.22 and an acceptance angle of 25°.

3. Results and discussion

3.1. Catalytic characterization. Figure 1 presents the characterization results for the silica catalyst sample employed in this work. The scanning electron microscopy (SEM) image of the SiO_2 (**Fig. 1(a)**) and the Co/SiO_2 (**Fig. 1(b)**) indicates the presence of spherical particles surrounded by shapeless agglomerations. It is indicated that the spherical morphology is the most stable shape achieved in nature [42]. Being used as catalysts for chemical reactions, spherical structures provide high mechanical strength, short pathways for diffusion of species, dispersion enhancement due to the stabilization of electrostatic charges, and high surface area to volume ratio [43-45]. The presence of such spherical particles in the catalysts is expected to promote the ammonia synthesis yield. The impregnation of metals i.e., Co on the SiO_2 did not alter the morphology of the silica significantly (**Fig. 1(b)**). The X-ray diffraction (XRD) reveals only a broad peak at 2θ of 26.08 º (JCPDS 05–0492), implying the amorphous structure of the silica (**Fig. 1(c)**). The SiO_2-related diffraction peak area was smaller in the impregnated catalysts. This is due to the competition with the sharp diffraction peaks of metals (Ag, Co, and Cu) in the approximate regions. Moreover, the diffraction peaks of Ag (JCPDS #04-0783), Co_3O_4 (JCPDS #42-1467), and CuO (JCPDS #80-1916) were well-detected from the Ag/SiO_2, Co/SiO_2, and Cu/SiO_2 catalysts, respectively. The ICP-OES of the Co/SiO_2, Ag/SiO_2, and Cu/SiO_2 catalysts verified the respective metallic content was 3.02, 3.10, and 3.04%, respectively. The Raman spectrum was collected from 1000 – 3500 cm^{-1} wavelengths for all catalyst samples (**Fig. 1(d)**). The peak at 1000 to 1300 cm^{-1} are associated with Si while the peaks at 1500 – 1600 cm^{-1} are assigned to the photoluminescence of interstitial oxygen from atmospheric air in the interparticle space, respectively.[46-48] Such interstitial oxygen lead to the formation of a Frenkel defect pair (Si–Si bond and interstitial oxygen atom, O) by dense electronic excitation. There are unknown peaks appearing between 2500 and 3000 cm^{-1}. These bands appear with the laser excitation (λ_{exc}) at 514.5 nm possibly due to either linearly coordinated resonance phenomena [49] or the presence of small amounts of carbon, derived

from organic surfactants employed during catalyst preparation, attributed to incomplete removal after calcination in air.

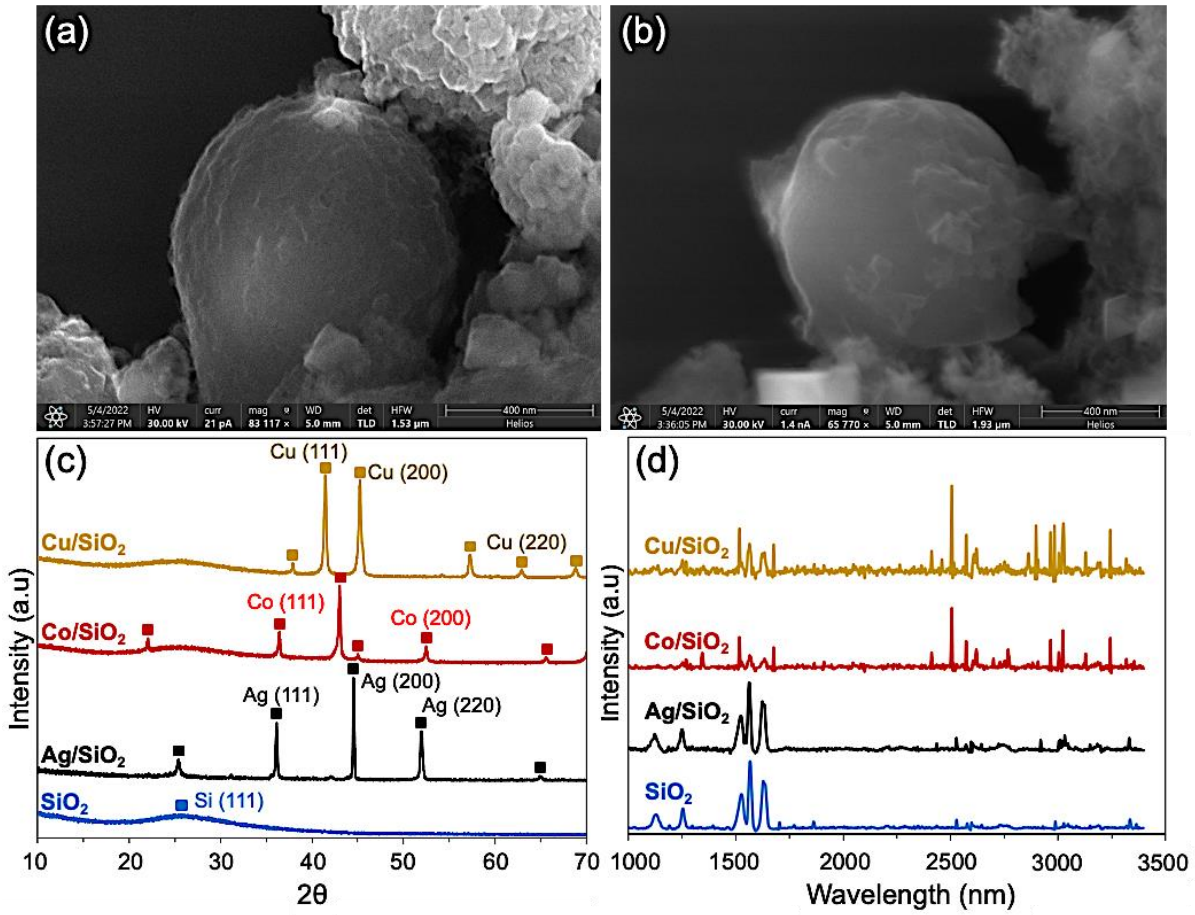

Fig. 1. (a) SEM image of the SiO_2 and **(b)** Co/SiO_2; **(c)** XRD patterns and **(d)** Raman spectrum of all prepared catalysts.

3.2. Catalytic activity. We studied the catalytic performance by screening the ammonia synthesis rate (r_{NH_3}) over plasma-driven ammonia synthesis from N_2/sea water vapor with various N_2 flowrates i.e., 3.1, 6.2, 12.5, and 25.0 sccm and plasma powers (2, 3, 5, and 6 W) in the absence of catalyst and ammonia was not detected. In contrast, an ammonia synthesis rate (r_{NH_3}) of 0.8 mmol.g_{cat}^{-1}.h^{-1} was obtained from a N_2/H_2 mixture at similar testing conditions (N_2 flowrate was 12.5 sccm and H_2 flowrate was fixed at 12.5 sccm, plasma power of 2 W), which is consistent with our previous studies [25, 30]. This result provides evidence that a catalyst is required for ammonia production from N_2 and sea water vapor. The observed

ammonia synthesis rate (r_{NH_3}) produced from N_2/sea water vapor mixture at different flowrates and plasma powers over the silica sphere catalyst is shown in **Fig. 2(a)**. The ammonia synthesis rate obtained from the N_2/H_2 system (H_2 flowrate fixed at 12.5 sccm, is shown in (**Fig. 2(b)**) over the silica catalyst was also performed to benchmark and compare the catalytic activity. We observed that ammonia could be produced effectively from sea water vapor and N_2 over the SiO_2 catalyst at the relatively low N_2 feed flowrate of 3.1 sccm, as shown in **Fig. 2(a)**. At this N_2 flowrate and an input plasma power of 2 W, 1.8 $mmol.g_{cat}^{-1}.h^{-1}$ of ammonia was produced from N_2/sea water vapor system while the highest ammonia synthesis rate could be obtained at the feed flowrate of 6.2 sccm with a value of 2.8 $mmol.g_{cat}^{-1}.h^{-1}$. Noticeably, at similar conditions, an ammonia synthesis rate of 2.6 $mmol.g_{cat}^{-1}.h^{-1}$ was obtained from the N_2/H_2 system with the N_2 flowrate of 3.1 sccm corresponding to the N_2:H_2 ratio of approximately 4.0 (H_2 was fixed at 12.5 sccm), as shown in **Fig. 2(b)**. The increase in the plasma power above 2 W, such as 3W, 5W, and 6 W, led to an enhancement in the ammonia synthesis rate when using N_2/H_2 mixture relative to N_2/sea water vapor (**Fig. 2(a)**&**(b))**. Accordingly, the highest ammonia synthesis rate (r_{NH_3}) value reached was approximately 5.0 $mmol.g_{cat}^{-1}.h^{-1}$, 1.5 times higher than that produced from N_2/sea water vapor system with 3.2 $mmol.g_{cat}^{-1}.h^{-1}$ at similar plasma power of 6 W. Ammonia could not be detected from the reaction of N_2/sea water vapor in the absence of catalyst, even when varying the plasma power. This result reveals that plasma power has less significant role in ammonia production from N_2/sea water vapor system than that of the catalyst, which played an important factor to secure a desirable ammonia synthesis rate. This also show experimentally the importance of the plasma-catalyst synergism when employing sea water vapor as hydrogen feedstock. These primary observations reveal novel directions for future work on optimizations of scalable ammonia production from cheap and widely available sources of "gold hydrogen" such as sea water. Moreover, the increment in the N_2 input flowrates above 6.1 sccm such as 12.5 and 25.0 sccm resulted in the subsequent decline of the ammonia synthesis rate (r_{NH_3}) produced from

N_2 and sea water vapor. Similarly, the ammonia synthesis rate (r_{NH_3}) produced from the N_2/H_2 system also reduced with the increase in the N_2 input flowrate (**Fig. 2(b)**). Moreover, we observed that the ammonia synthesis rate produced from the N_2/sea water vapor system was in range of that obtained over the N_2/pure water vapor system (**Fig. S3**) at similar testing conditions and catalysts. As an example, the maximum ammonia synthesis rate with Co/SiO_2 for pure water vapor was 3.9 $mmol.g_{cat}^{-1}.h^{-1}$ compared to the value obtained for the same catalyst with sea water vapor of 3.7 $mmol.g_{cat}^{-1}.h^{-1}$ at a N_2 flow rate of 6.1 sccm and 2 W. The potential to use seawater instead of pure water is advantageous in a commercial process because of its wide availability. Such observations prove a great potential for further optimization of ammonia production process from N_2 and sea water for industrial scale. However, further details related to the long-term operation of equipment with sea water should be detailed in future studies due to the corrosion, a process caused by saltwater reacting to metals. Energy yield produced from both N_2/sea water vapor and N_2/H_2 mixtures declined with the increase of input power. Ammonia synthesis from the N_2/sea water vapor at the N_2 input flowrate of 6.2 sccm secured a higher energy yield (2.3 $g_{NH_3}.kW^{-1}.h^{-1}$) than that produced with greater N_2 flowrates such as 12.5 sccm (2.2 $g_{NH_3}.kW^{-1}.h^{-1}$) and 25.0 sccm (0.6 $g_{NH_3}.kW^{-1}.h^{-1}$), as shown in (**Fig. 2(c)**. (Calculation details can be found in Supporting Information). Meanwhile, the highest energy yield for the synthesis of ammonia over the N_2/H_2 mixture was 2.2 $g_{NH_3}.kW^{-1}.h^{-1}$ at a N_2 flowrate of 3.1 sccm (**Fig. 2(d))**.

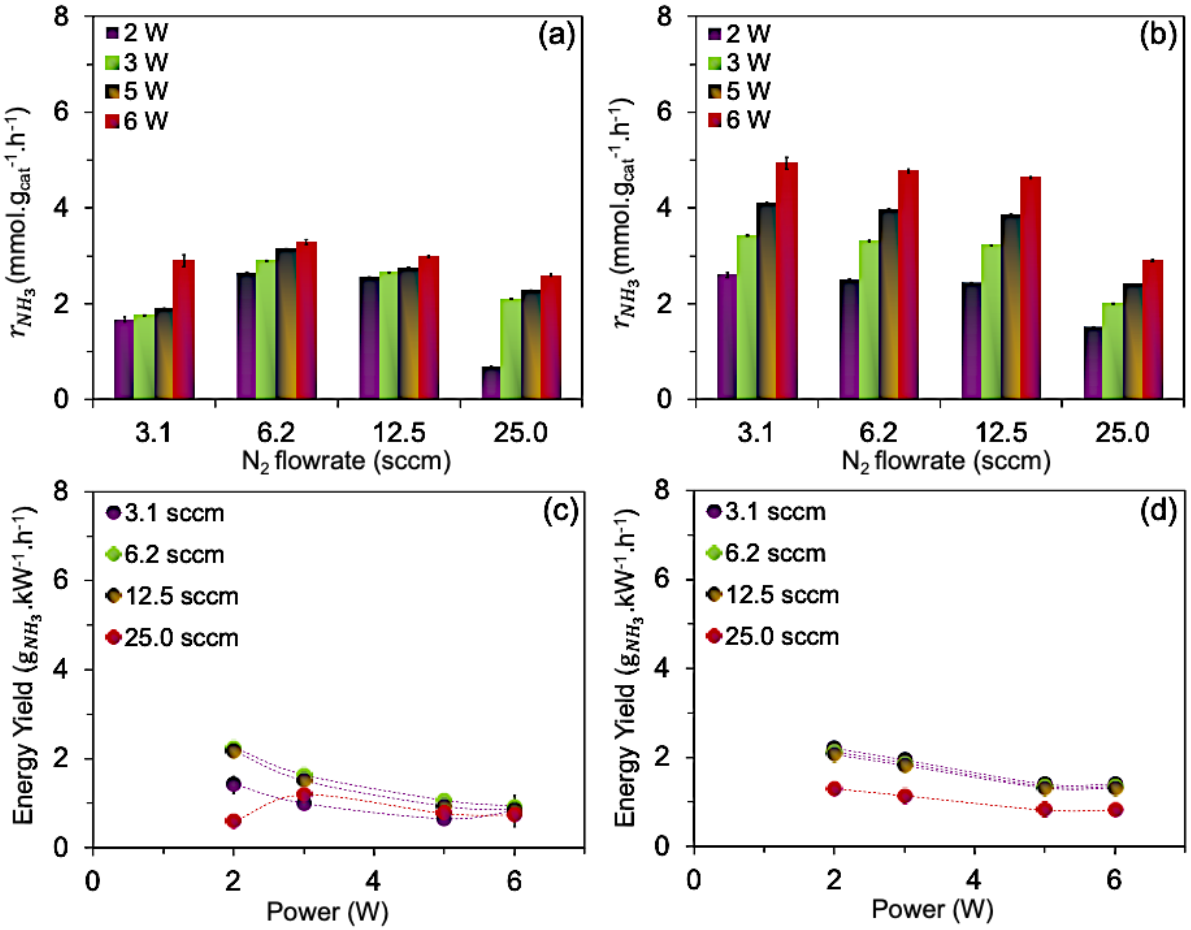

Fig. 2. Ammonia synthesis rate (r_{NH_3}) produced from **(a)** N_2/sea water vapor and **(b)** N_2/H_2; Energy yield obtained from **(c)** N_2/sea water vapor and **(d)** N_2/H_2 over the SiO_2 catalyst at different plasma powers.

These observations further validate our postulate that plasma catalytic reactions for ammonia production from N_2 and sea water vapor and N_2/H_2 were not solely controlled by the plasma power but by the nature of the catalyst as well. The presence of a catalyst in the plasma zone appears to alter the plasma-surface reactions, resulting in plasma-catalyst synergism,[50] and by that, promoting the ammonia production. To verify the influence of the metal active centers on ammonia synthesis from N_2 and sea water vapor, this work also employed the SiO_2 as a support impregnated with metals such as Ag, Cu, and Co. The catalytic performance of these catalysts is shown in **Fig. 3**. For the N_2 and sea water vapor system, the presence of a metal supported on the SiO_2 support did not increase the ammonia synthesis rate significantly. Accordingly, the Co/SiO_2 sample produced 3.8 mmol.g_{cat}^{-1}.h^{-1} of ammonia while the Ag/SiO_2

and Cu/SiO_2 delivered an ammonia production rate of 3.4 and 3.3 $mmol.g_{cat}^{-1}.h^{-1}$ with the N_2 input flowrate of 6.2 sccm and power of 2 W, respectively (**Fig. 3(a)**). All these values are within range of each other despite the type of metal employed. When comparing with other researchers, [33, 34] who have reported to produce ammonia from water, the synthesis rate of 2.67 mmol g_{cat}^{-1} h^{-1} from N_2/water has been observed over the noble catalyst Ru/MgO at a N_2 feed of 100 sccm and V_{p-p} of 8.23 kV. From our prepared catalysts, Co/SiO_2, displays a comparative performance in terms of ammonia synthesis rate when employing N_2 and sea water vapor at a N_2 feed of 6.2 sccm and power of 2 W (about V_{p-p} of 4.12 kV) with a value of 3.7 mmol g_{cat}^{-1} h^{-1}. An advantage, with respect to these reports is that a transition metal-based catalyst such as Co/SiO_2 is lower in cost and there is a wider availability compared to noble metals such as Ru [10]. However, for the N_2 sea water vapor system is important to remember the challenging selectivity competition with N_2O formation due to the oxygen presence related to the hydrogen source. This can explain the apparent no effect of the metal towards ammonia production.

Noticeably, for the N_2/H_2 reaction mixture the presence of the Co/SiO_2 catalyst promoted the ammonia synthesis rate (r_{NH_3}) to 6.3 $mmol.g_{cat}^{-1}.h^{-1}$, which is threefold to that produced over the SiO_2 support at similar experimental conditions (**Fig. 3(b)**). In general, the N_2/H_2 reaction mixture observed a greater impact from the metal content compared to the case when the sea water vapor is employed as hydrogen source. Besides, the metallic active centers possessing better activity than oxides like silica, with the possibility to delivered better ammonia production rate [51], since the selectivity competition with N_2O does not exist in this case.

From the catalysts employed the Co/SiO_2 catalyst displayed the highest energy yield of 3.2 and 5.3 $g_{NH_3}.kW^{-1}.h^{-1}$ for ammonia synthesis over the N_2/sea water vapor and N_2/H_2 systems respectively at a power of 2 W (**Fig. 3(c) & (d)**). The Ag/SiO_2 and Cu/SiO_2 delivered energy yields of 2.7 and 5.0 $g_{NH_3}.kW^{-1}.h^{-1}$ obtained from the N_2/sea water vapor and N_2/H_2 systems, respectively. These results confirmed the important role of the catalysts in the synthesis of

ammonia and the possible need of different catalysts when switching the hydrogen source for this reaction due to the added presence of oxygen.

In terms of materials, the Co/SiO_2 catalyst also exhibited the highest ammonia production rate at all testing conditions (**Fig. S4**&**S5**). This can be attributed to the lower binding energy of Co with nitrogen relative to the Ag and Cu [52, 53]. Other researchers have also indicated that metals having stronger nitrogen binding energy delivered lower ammonia synthesis rate due to slow N-H formation [54-56]. Accordingly, the theoretical targeted ammonia synthesis yield for an ideal small scale ammonia synthesis process is 100 $g_{NH_3}.kW^{-1}.h^{-1}$, while the currently reported values employing N_2/H_2 are mostly below 20 $g_{NH_3}.kW^{-1}.h^{-1}$ produced over noble catalysts i.e., Ru-based catalysts. [53] Other catalysts such as Ni or Fe are reported to produce energy yield of below 1.0 $g_{NH_3}.kW^{-1}.h^{-1}$.[57] In comparison with such reported works, the ammonia energy yield obtained from either N_2/sea water vapor (3.2 $g_{NH_3}.kW^{-1}.h^{-1}$) or N_2/H_2 system (5.6 $g_{NH_3}.kW^{-1}.h^{-1}$) over the Co/SiO_2 catalyst in this work displays a competitive performance and high potential for further optimizations.

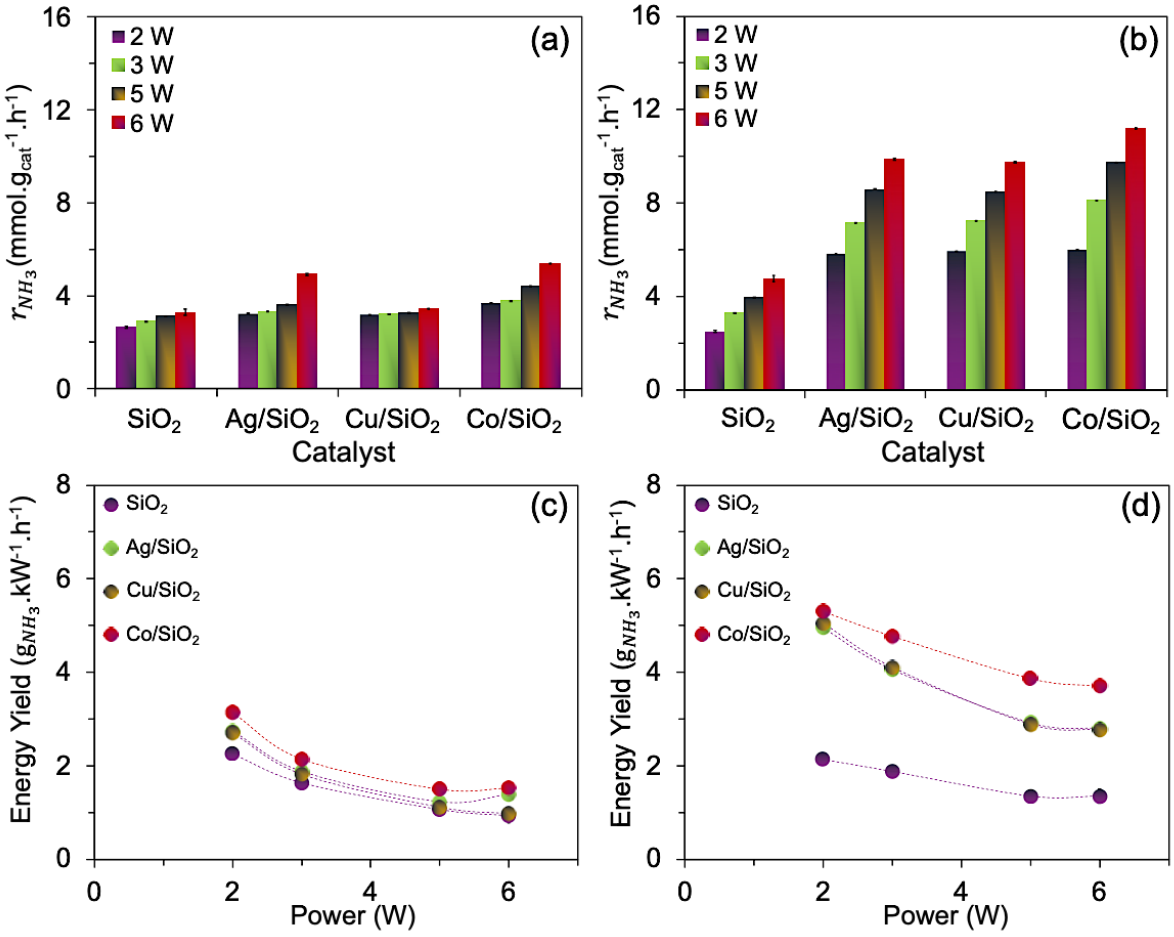

Fig. 3. Ammonia synthesis rate (r_{NH_3}) produced from **(a)** N_2/sea water vapor and **(b)** N_2/H_2; Energy yield obtained from ammonia synthesis reaction of **(c)** N_2/sea water vapor and **(d)** N_2/H_2 at different plasma powers and an input N_2 flowrate of 6.2 sccm.

3.3. In situ OES. It should be noticed that the inevitable obstacle for the substitution of H_2 by oxygen-contained reactants i.e., seawater is the formation of oxidative species as by-products such as nitrogen oxides. In this work, operando optical emission spectroscopy (OES) analysis was performed to study the plasma excitation process with and without catalyst. The results are shown in **Fig. 4.** The overall OES spectrum for ammonia synthesis from different routes are well-detected (**Fig. 4(a)**). Noticeably, the main nitrogen oxide product detected was nitrous oxide (N_2O), as shown in (**Fig. 4(b)**). Other nitrogen oxides such as N_xO_y were possibly generated but within concentrations below detection limits. Compared with the plasma-only experiments, the catalyst-plasma experiment for ammonia synthesis from N_2 and sea water vapor exhibited insignificant differences in the intensity of the N_2O-related peaks (**Fig. 4(b)**).

However, its intensity was higher than that of the ammonia synthesis route from N_2 and H_2. Such observations indicate that N_2O formation might occur predominantly in the gas phase and is promoted with the presence of sea water vapor.[58] Noticeably, NH_x-assigned peak at 336.1 nm was well-detected from the plasma catalyst processes with N_2/H_2 and N_2/sea water vapor while it is not visible for the plasma-only process with N_2/sea water vapor (**Fig. 4(c)**). This result validates the absence of ammonia product from N_2/sea water vapor over the plasma-only route as discussed previously. In addition, plasma-activated nitrogen species exist in the form of vibrational and rotational excitation, electronic excitation, and ionization without minimal dissociation observed (**Fig. 4(d)**).

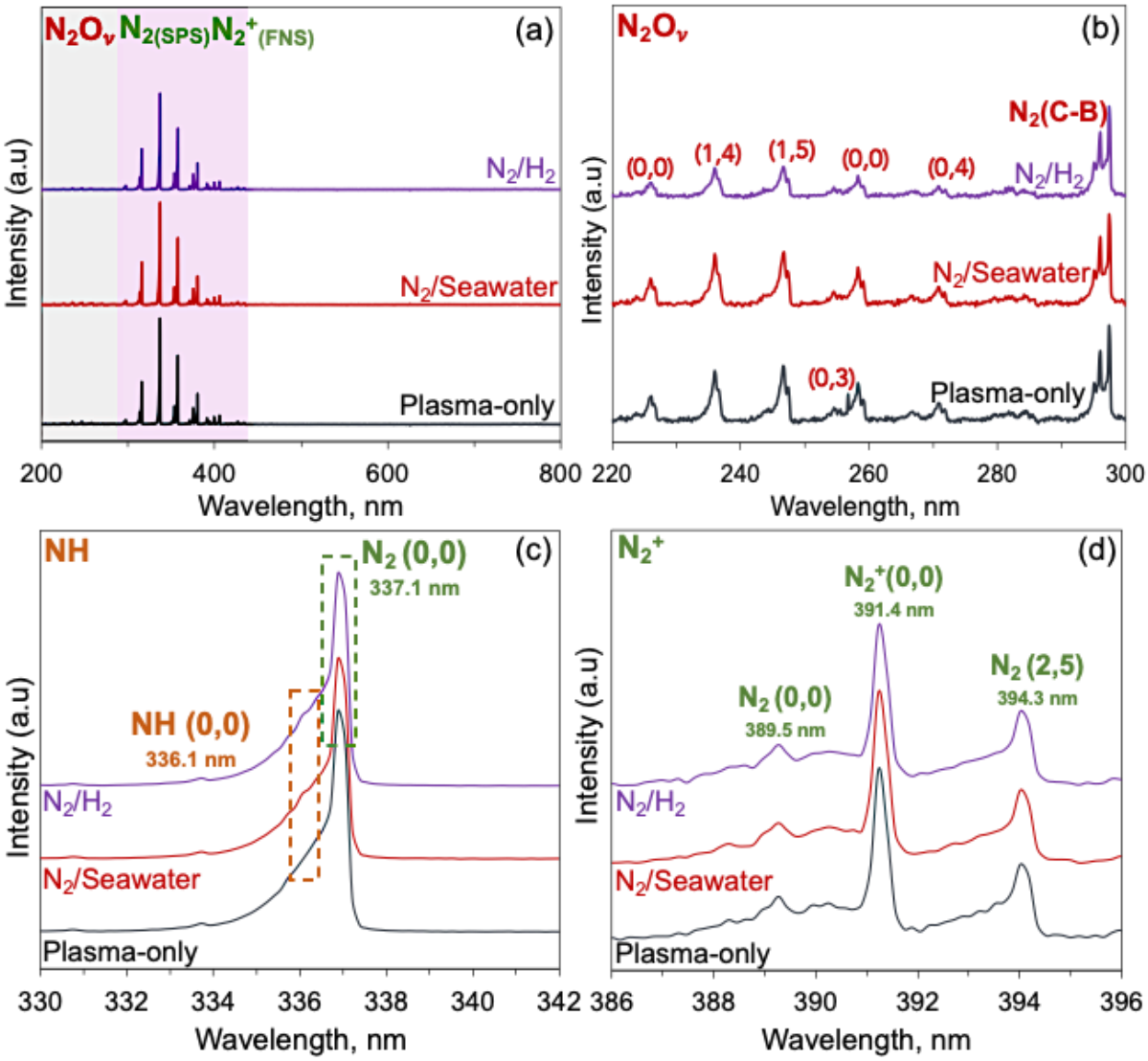

Fig. 4. (a) Overall OES spectrum (200-800 nm) for plasma-assisted catalytic ammonia synthesis from N_2/H_2, N_2/sea water vapor, and plasma without catalyst (plasma-only) of ammonia synthesis reaction from N_2/sea water vapor; **(b)** zoom-in OES spectrum of $NO_{(\gamma)}$ (220-300 nm); **(c)** zoom-in OES spectrum of NH (330-342 nm); and **(d)** zoom-in OES spectrum of N_2^+ (386-396 nm) obtained over the Co/SiO_2 catalyst.

Noticeably, the OES spectrum collected from the ammonia synthesis reactions over the Co/SiO_2 catalyst (**Fig. 5**) displayed the presence of N_2O, similar to the one obtained over the SiO_2 catalyst. Meanwhile, nitrous oxides were not detected from the reaction over the Ag/SiO_2. By experimental data and computational calculations, Kepp et al.,[59] have indicated that metal-oxygen interactions are in an order of Co, Cu, and Ag with bond dissociation enthalpy with oxygen of 420, 310, and 200 kJ/mol, respectively. Given stronger affinity to oxygen, more active oxygen was absorbed on the Co/SiO_2 surface and reacted with N_2^* to form nitrous oxide while the reactions occurred over the Cu/SiO_2 presented weak intensity of nitrous oxide, as shown in **Fig. 5**. For the metals with weaker affinity such as Ag or Cu, active oxygen was possibly prone to recombination with H atoms. These conclusions can be verified via the selectivity of N_2O and NH_3 (**Fig. S6**). The N_2O calibration curve is also shown in **Fig. S7**. At N_2 input flowrate of 6.2 sccm and 6 W, the Ag/SiO_2 and Co/SiO_2 catalysts displayed lower N_2O selectivity of 27.5 and 32.0%, respectively than that of the SiO_2 and the Cu/SiO_2, which produced the N_2O selectivity of 47.6 and 41.8%, respectively (**Eq.(3)**, Supporting Information).

In terms of nitrogen fixation, such nitrogen oxide can be a useful platform for other chemicals production. A possible concept to make a full use of downstream products from ammonia synthesis is the addition of a membrane DBD plasma reactor to separate produced N_2O for other chemical synthesis i.e., HNO_3 with air while the formed ammonia can be liquefied. This product separation strategy in a DBD reactor has been explored by our group for the N_2/H_2 plasma ammonia synthesis [25]. Another solution is to recycle the formed NO_x to the reactor

for ammonia synthesis [60]. A possible concern is whether a desalination step is necessary to translate seawater to purer water prior to entering to the DBD reactor for ammonia synthesis reaction. This is originated from an apprehension that seawater possibly causes oxidation of the electrode of the DBD reactor. Nevertheless, even though either pure water or air was used, the inner electrode of the DBD reactor also deals with oxidative issues under long-term cycling reactions. Such phenomenon requires a thoughtful study to assess the effects of oxygen-consisted co-reactants such as pure water, seawater, or air, which is out of the main scope of this work. While experimental results of this work indicated insignificant difference of ammonia production rate from both N_2/pure water vapor and N_2/sea water vapor, the addition of such desalination step into the process undoubtedly raises investment capital. Future work in this area can focus on the development of highly active catalysts, process optimization, and evaluation of scale-up capacity with a vision to propose a feasible technology for ammonia production plants at harbours or remote sea areas.

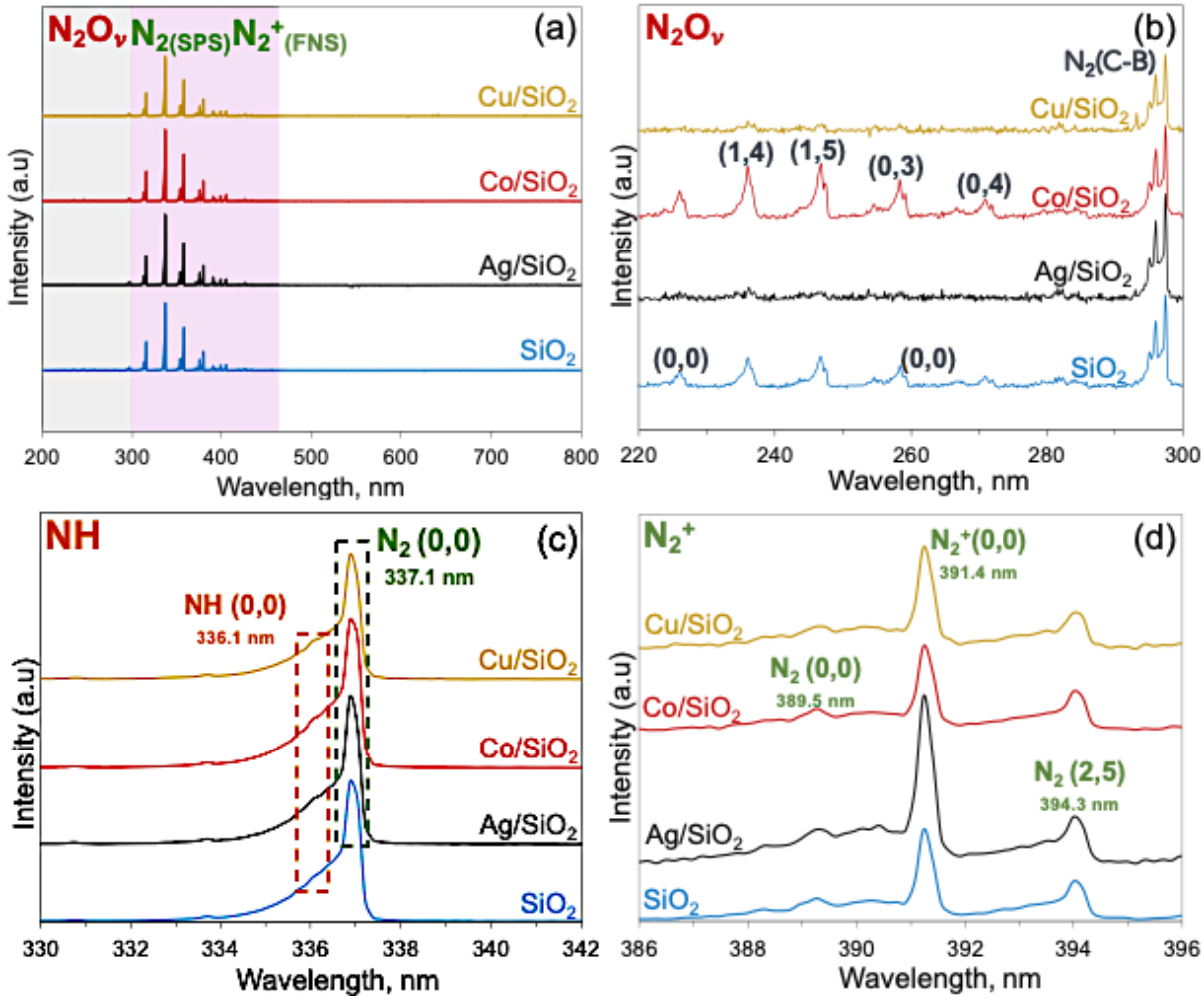

Fig. 5. (a) Overall OES spectrum (200-800 nm) for plasma-assisted catalytic ammonia synthesis from N_2/sea water vapor, **(b)** zoom-in OES spectrum of $NO_{(v)}$ (220-300 nm); **(c)** zoom-in OES spectrum of NH (330-342 nm); and **(d)** zoom-in OES spectrum of N_2^+ (386-396 nm) of different catalysts. The OES spectrum of the SiO_2 catalyst is re-presented for comparison purpose.

Insights on the plasma ammonia pathway from sea water vapor and N_2 plasma activation. Despite the recent developments and progress in understanding the plasma-mediated ammonia synthesis from N_2 and H_2 [24, 61, 62] there is still much to be done. At the same time, the use of novel hydrogen sources such as seawater is expected to alter these proposed reaction pathways [63]. This work seeks to provide plausible pathway insights into the plasma activation of N_2 and sea water vapor for ammonia production. Experimental results of this work indicated that ammonia was not detected from the reaction between N_2 and sea water vapor

with no catalyst. Therefore, it is worthwhile to mention that a catalyst is needed to provide an active surface for plasma activated N_2 species to react with H* species dissociated from H_2O vapor. Other researchers also reveal that an active surface is necessary to secure a good ammonia synthesis rate [57]. DBD plasma offers a high degree of excitation (vibrational or electronic) however it observes a low degree of dissociation [64]. Some researchers also indicate the possibility that N_2 is not completely dissociated in the plasma environment and the presence of a heterogeneous catalyst could facilitate the dissociation of the plasma-generated species [51]. However, recent experimental-theoretical work from our group shows the importance of N radicals as they are more reactive compared to N vibrational species. And even a minute presence of N radicals can offer a pivotal effect in the synthesis of ammonia from N_2 and H_2.[65] However, most of the reported mechanisms for ammonia synthesis from N_2 and H_2 include the formation of plasma-induced vibrationally excited $N_{2(v)}$ species and the excitation of adsorbed $N_{(ads)}$ on the catalyst surface to react with H_2 to form NH_3 *via* either Eley-Rideal (E-R) or Langmuir-Hinshelwood (L-H)[23, 61, 62, 65-67]. With both the E-R and L-H mechanisms involved in many reactions to form ammonia. Meaning either N radicals or N vibrational species can be disregarded as both play a role in the ammonia synthesis reactions. However, the presence of seawater alters such mechanisms by adding the excitation and/or ionization of water molecules. In our case, the nitrogen plasma can react with H_2O vapor molecules to generate NH and OH radicals [68] where the extraction of H from water molecules plays an important role in the formation of ammonia. This deduction is in good agreement with other researchers [69, 70]. In this work H_2O vapor molecules could cause the quenching of N_2 vibrational levels given the N_2/H_2O vibrational-translational relaxation, reducing electron density. This added to the consumption of nitrogen excited species to form N_2O reduces the overall ammonia synthesis rate [71]. OH* could also be generated from the dissociation of H_2O molecules. Nevertheless, the presence of such OH* species would lead to the formation of H_2O_2,[72] which was not detected in this work. Therefore, such hydroxyl radicals with

significant short life could get dissociated to H* and O* subsequently. Experimental results in this work indicated that even if the Co/SiO_2 catalyst displayed good ammonia synthesis rate, a strongest N_2O-related spectra was detected, indicating the strong competition imposed by N_2O formation. While the Ag/SiO_2 catalyst displayed no OES spectra related to NO_x species it showed a competitive activity relative to the Co/SiO_2, as discussed previously. Meaning the surface interactions might be overcoming the gas events. This also shows the importance of the silica substrate that as mentioned above can aid in the N_2O decomposition. Hence, future work can focus on enhancement of the catalytic activity of oxygen-phobic metals or electron density on the catalyst surface to dissociate N_2 and maintain relatively weak intermediate bindings effectively. Such active metals would be ideal if they possess high affinity to oxidative oxygen species to offer strong bindings or act as oxygen sinks [73, 74] to hinder the formation of nitrogen oxide.

A schematic diagram describing a plausible reaction pathway for ammonia synthesis from N_2 and sea water vapor is shown below in **Fig. 6**.

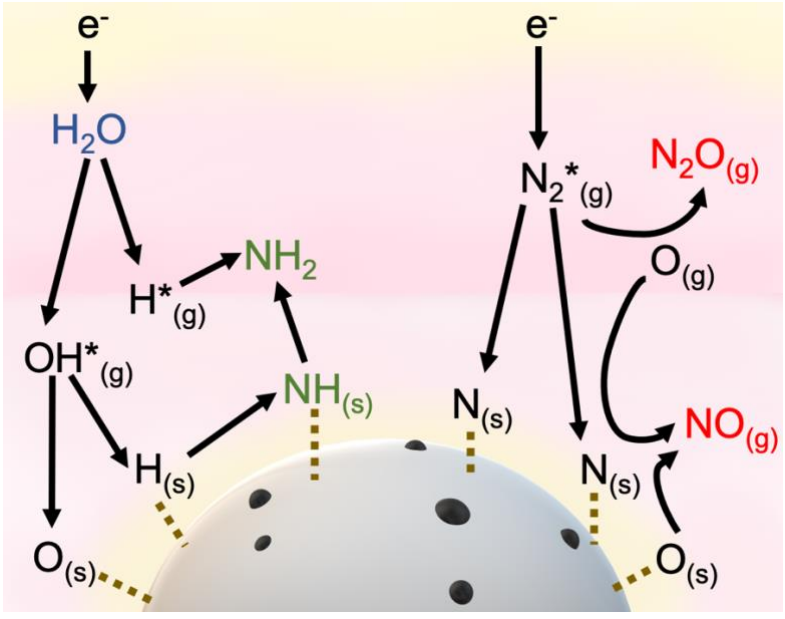

Fig. 6. Schematic diagram of the plausible pathway of plasma-driven ammonia synthesis from N_2 and sea water vapor over the metal supported on SiO_2 catalyst.

4. Conclusions

In this work, ammonia was successfully produced from N_2 and sea water vapor at ambient conditions directly from using renewable sources such as N_2, sea water vapor, and electricity potentially from solar or wind. The presence of a catalyst was required to secure the formation of ammonia from the N_2/sea water vapor. An ammonia synthesis rate of 2.8 $mmol.g_{cat}^{-1}.h^{-1}$ and an energy efficiency of 2.3 $g_{NH_3}.kW^{-1}.h^{-1}$ could be produced from N_2/sea water vapor reaction with a N_2 flowrate of 6.2 sccm and a relatively low plasma input power of 2 W over the SiO_2. The use of seawater as an alternative H_2 source delivered a comparative ammonia production rate and energy yield relative to the utilization of pure H_2. Plasma power has a less significant role in ammonia production relative to the catalyst that acted as an important factor to secure a desirable ammonia synthesis rate. This work can open novel research directions for future work to rationally design active metals supported on silica or other good dielectric materials like perovskites for ammonia production from seawater sustainably and economically.

Declaration of Competing Interest

The authors declare that they have no known competing financial interests or personal relationships that could have appeared to influence the work reported in this paper.

Appendix A. Supplementary data

Supporting Information can be found online at.

Acknowledgements

Maria L. Carreon acknowledges the support from NSF CBET Award No. 2203166 and grant No. DE-SC0023261, U.S. DEPARTMENT OF ENERGY, Basic Research.

References

[1] L. Ye, H. Li, K. Xie, Sustainable ammonia production enabled by membrane reactor, Nature Sustainability, (2022).

[2] G. Jeerh, M. Zhang, S. Tao, Recent progress in ammonia fuel cells and their potential applications, Journal of Materials Chemistry A, 9 (2021) 727-752.

[3] J. Kim, C. Huh, Y. Seo, End-to-end value chain analysis of isolated renewable energy using hydrogen and ammonia energy carrier, Energy Conversion and Management, 254 (2022) 115247.

[4] D.W. Kang, J.H. Holbrook, Use of NH_3 fuel to achieve deep greenhouse gas reductions from US transportation, Energy Reports, 1 (2015) 164-168.

[5] X. Xu, E. Liu, N. Zhu, F. Liu, F. Qian, Review of the current status of ammonia-blended hydrogen fuel engine development, Energies, 15 (2022) 1023.

[6] C. Kurien, M. Mittal, Review on the production and utilization of green ammonia as an alternate fuel in dual-fuel compression ignition engines, Energy Conversion and Management, 251 (2022) 114990.

[7] Y. Liu, C.W. Wang, X.F. Xu, B.W. Liu, G.M. Zhang, Z.W. Liu, Q. Chen, H.B. Zhang, Synergistic effect of Co–Ni bimetal on plasma catalytic ammonia synthesis, Plasma Chemistry and Plasma Processing, 42 (2022) 267-282.

[8] X. Zhu, J. Liu, X. Hu, Z. Zhou, X. Li, W. Wang, R. Wu, X. Tu, Plasma-catalytic synthesis of ammonia over Ru-based catalysts: Insights into the support effect, Journal of the Energy Institute, 102 (2022) 240-246.

[9] H. Zhao, G. Song, Z. Chen, X. Yang, C. Yan, S. Abe, Y. Ju, S. Sundaresan, B.E. Koel, In situ identification of NNH and N_2H_2 by using molecular-beam mass spectrometry in plasma-assisted catalysis for NH_3 synthesis, ACS Energy Letters, 7 (2022) 53-58.

[10] H.M. Nguyen, J. Sunarso, C. Li, G.H. Pham, C. Phan, S. Liu, Microwave-assisted catalytic methane reforming: A review, Applied Catalysis A: General, 599 (2020) 117620.

[11] A. Oni, K. Anaya, T. Giwa, G. Di Lullo, A. Kumar, Comparative assessment of blue hydrogen from steam methane reforming, autothermal reforming, and natural gas decomposition technologies for natural gas-producing regions, Energy Conversion and Management, 254 (2022) 115245.

[12] J. Sun, D. Alam, R. Daiyan, H. Masood, T. Zhang, R. Zhou, P.J. Cullen, E.C. Lovell, A.R. Jalili, R. Amal, A hybrid plasma electrocatalytic process for sustainable ammonia production, Energy & Environmental Science, 14 (2021) 865-872.

[13] E.C. Oliver, M.G. Donat, M.T. Burrows, P.J. Moore, D.A. Smale, L.V. Alexander, J.A. Benthuysen, M. Feng, A. Sen Gupta, A.J. Hobday, Longer and more frequent marine heatwaves over the past century, Nature communications, 9 (2018) 1-12.

[14] R. Hawtof, S. Ghosh, E. Guarr, C. Xu, R. Mohan Sankaran, J.N. Renner, Catalyst-free, highly selective synthesis of ammonia from nitrogen and water by a plasma electrolytic system, Science advances, 5 (2019) eaat5778.

[15] J. Zheng, Y. Lyu, M. Qiao, R. Wang, Y. Zhou, H. Li, C. Chen, Y. Li, H. Zhou, S. Wang, Photoelectrochemical synthesis of ammonia on the aerophilic-hydrophilic heterostructure with 37.8% efficiency, Chem, 5 (2019) 617-633.

[16] H. Patel, R.K. Sharma, V. Kyriakou, A. Pandiyan, S. Welzel, M.C.M. van de Sanden, M.N. Tsampas, Plasma-activated electrolysis for cogeneration of nitric oxide and hydrogen from water and nitrogen, ACS Energy Letters, 4 (2019) 2091-2095.

[17] R.K. Sharma, H. Patel, U. Mushtaq, V. Kyriakou, G. Zafeiropoulos, F. Peeters, S. Welzel, M.C.M. van de Sanden, M.N. Tsampas, Plasma activated electrochemical ammonia synthesis from nitrogen and water, ACS Energy Letters, 6 (2021) 313-319.

[18] Z. Zhou, Z. Pei, L. Wei, S. Zhao, X. Jian, Y. Chen, Electrocatalytic hydrogen evolution under neutral pH conditions: current understandings, recent advances, and future prospects, Energy & Environmental Science, 13 (2020) 3185-3206.

[19] P. Peng, C. Schiappacasse, N. Zhou, M. Addy, Y. Cheng, Y. Zhang, K. Ding, Y. Wang, P. Chen, R. Ruan, Sustainable non-thermal plasma-assisted nitrogen fixation—synergistic catalysis, ChemSusChem, 12 (2019) 3702-3712.

[20] Y. Sun, J. Wu, Y. Wang, J. Li, N. Wang, J. Harding, S. Mo, L. Chen, P. Chen, M. Fu, D. Ye, J. Huang, X. Tu, Plasma-catalytic CO_2 hydrogenation over a Pd/ZnO catalyst: In situ probing of gas-phase and surface reactions, JACS Au, (2022).

[21] G. Chen, X. Tu, G. Homm, A. Weidenkaff, Plasma pyrolysis for a sustainable hydrogen economy, Nature Reviews Materials, 7 (2022) 333-334.

[22] J. Sun, D. Alam, R. Daiyan, H. Masood, T. Zhang, R. Zhou, P.J. Cullen, E.C. Lovell, A. Jalili, R. Amal, A hybrid plasma electrocatalytic process for sustainable ammonia production, Energy & Environmental Science, 14 (2021) 865-872.

[23] K.H.R. Rouwenhorst, H.G.B. Burbach, D.W. Vogel, J. Núñez Paulí, B. Geerdink, L. Lefferts, Plasma-catalytic ammonia synthesis beyond thermal equilibrium on Ru-based catalysts in non-thermal plasma, Catalysis Science & Technology, 11 (2021) 2834-2843.

[24] Y. Wang, M. Craven, X. Yu, J. Ding, P. Bryant, J. Huang, X. Tu, Plasma-enhanced catalytic synthesis of ammonia over a Ni/Al_2O_3 catalyst at near-room temperature: Insights into the importance of the catalyst surface on the reaction mechanism, ACS Catalysis, 9 (2019) 10780-10793.

[25] F. Gorky, H.M. Nguyen, J.M. Lucero, S. Guthrie, J.M. Crawford, M.A. Carreon, M.L. Carreon, CC3 porous organic cage crystals and membranes for the non-thermal plasma catalytic ammonia synthesis, Chemical Engineering Journal Advances, (2022) 100340.

[26] H.M. Nguyen, M.L. Carreon, Non-thermal plasma-assisted deconstruction of high-density polyethylene to hydrogen and light hydrocarbons over hollow ZSM-5 microspheres, ACS Sustainable Chemistry & Engineering, 10 (2022) 9480-9491.

[27] S. Gershman, H. Fetsch, F. Gorky, M.L. Carreon, Identifying regimes during plasma catalytic ammonia synthesis, Plasma Chemistry and Plasma Processing, 42 (2022) 731-757.

[28] F. Gorky, J.M. Lucero, J.M. Crawford, B. Blake, M.A. Carreon, M.L. Carreon, Plasma-induced catalytic conversion of nitrogen and hydrogen to ammonia over zeolitic imidazolate frameworks ZIF-8 and ZIF-67, ACS Applied Materials & Interfaces, 13 (2021) 21338-21348.

[29] F. Gorky, J.M. Lucero, J.M. Crawford, B.A. Blake, S.R. Guthrie, M.A. Carreon, M.L. Carreon, Insights on cold plasma ammonia synthesis and decomposition using alkaline earth metal-based perovskites, Catalysis Science & Technology, 11 (2021) 5109-5118.

[30] F. Gorky, A. Best, J. Jasinski, B.J. Allen, A.C. Alba-Rubio, M.L. Carreon, Plasma catalytic ammonia synthesis on Ni nanoparticles: The size effect, Journal of Catalysis, 393 (2021) 369-380.

[31] J.R. Shah, F. Gorky, J. Lucero, M.A. Carreon, M.L. Carreon, Ammonia synthesis via atmospheric plasma catalysis: Zeolite 5A, a case of study, Industrial & Engineering Chemistry Research, 59 (2020) 5167-5176.

[32] J. Shah, F. Gorky, P. Psarras, B. Seong, D.A. Gómez-Gualdrón, M.L. Carreon, Enhancement of the yield of ammonia by hydrogen-sink effect during plasma catalysis, ChemCatChem, 12 (2020) 1200-1211.

[33] T. Zhang, R. Zhou, S. Zhang, R. Zhou, J. Ding, F. Li, J. Hong, L. Dou, T. Shao, A.B. Murphy, K. Ostrikov, P.J. Cullen, Sustainable ammonia synthesis from nitrogen and water by one-step plasma catalysis, Energy & Environmental Materials, n/a.

[34] J. Hong, T. Zhang, R. Zhou, S. Zhang, L. Dou, R. Zhou, B. Ashford, T. Shao, A. Murphy, K. Ostrikov, P.J. Cullen, Green chemical pathway of plasma synthesis of ammonia from nitrogen and water: a comparative kinetic study with N_2/H_2 system, Green Chemistry, (2022).

[35] C. Hess, R. Schlögl, Nanostructured catalysts: selective oxidations, Royal Society of Chemistry, 2011.

[36] T. Suttikul, T. Sreethawong, H. Sekiguchi, S. Chavadej, Ethylene epoxidation over alumina- and silica-supported silver catalysts in low-temperature AC dielectric barrier discharge, Plasma Chemistry and Plasma Processing, 31 (2011) 273-290.

[37] T. Norby, M. Widerøe, R. Glöckner, Y. Larring, Hydrogen in oxides, Dalton Transactions, (2004) 3012-3018.

[38] U. Wannagat, The silicon-nitrogen bond, in: G. Bendz, I. Lindqvist, V. Runnström-Reio (Eds.) Biochemistry of Silicon and Related Problems, Springer US, Boston, MA, 1978, pp. 77-90.

[39] F. Gorky, S.R. Guthrie, C.S. Smoljan, J.M. Crawford, M.A. Carreon, M.L. Carreon, Plasma ammonia synthesis over mesoporous silica SBA-15, Journal of Physics D: Applied Physics, 54 (2021) 264003.

[40] H.M. Choi, S.-J. Lee, S.-H. Moon, T.N. Phan, S.G. Jeon, C.H. Ko, Comparison between unsupported mesoporous Co_3O_4 and supported Co_3O_4 on mesoporous silica as catalysts for N_2O decomposition, Catalysis Communications, 82 (2016) 50-54.

[41] M. Piumetti, M. Hussain, D. Fino, N. Russo, Mesoporous silica supported Rh catalysts for high concentration N_2O decomposition, Applied Catalysis B: Environmental, 165 (2015) 158-168.

[42] H. Zhu, Z. Mao, B. Liu, T. Yang, X. Feng, H. Jin, C. Peng, C. Yang, J. Wang, X. Fang, Regulating catalyst morphology to boost the stability of Ni–Mo/Al_2O_3 catalyst for ebullated-bed residue hydrotreating, Green Energy & Environment, 6 (2021) 283-290.

[43] C. Pagis, A.R. Morgado Prates, D. Farrusseng, N. Bats, A. Tuel, Hollow zeolite structures: an overview of synthesis methods, Chemistry of Materials, 28 (2016) 5205-5223.

[44] W.C. Yoo, S. Kumar, Z. Wang, N.S. Ergang, W. Fan, G.N. Karanikolos, A.V. McCormick, R.L. Penn, M. Tsapatsis, A. Stein, Nanoscale reactor engineering: hydrothermal synthesis of uniform zeolite particles in massively parallel reaction chambers, Angewandte Chemie, 120 (2008) 9236-9239.

[45] H. Taghvaei, A. Moaddeli, A. Khalafi-Nezhad, A. Iulianelli, Catalytic hydrodeoxygenation of lignin pyrolytic-oil over Ni catalysts supported on spherical Al-MCM-41 nanoparticles: Effect of Si/Al ratio and Ni loading, Fuel, 293 (2021) 120493.

[46] L. Skuja, B. Güttler, D. Schiel, A.R. Silin, Quantitative analysis of the concentration of interstitial O_2 molecules in SiO_2 glass using luminescence and Raman spectrometry, Journal of Applied Physics, 83 (1998) 6106-6110.

[47] S. Agnello, D.D. Francesca, A. Alessi, G. Iovino, M. Cannas, S. Girard, A. Boukenter, Y. Ouerdane, Interstitial O_2 distribution in amorphous SiO_2 nanoparticles determined by Raman and photoluminescence spectroscopy, Journal of Applied Physics, 114 (2013) 104305.

[48] K. Kajihara, T. Miura, H. Kamioka, A. Aiba, M. Uramoto, Y. Morimoto, M. Hirano, L. Skuja, H. Hosono, Diffusion and reactions of interstitial oxygen species in amorphous SiO_2: A review, Journal of Non-Crystalline Solids, 354 (2008) 224-232.

[49] M. Ivanda, R. Clasen, M. Hornfeck, W. Kiefer, Raman spectroscopy on SiO_2 glasses sintered from nanosized particles, Journal of Non-Crystalline Solids, 322 (2003) 46-52.

[50] Y. Wang, W. Yang, S. Xu, S. Zhao, G. Chen, A. Weidenkaff, C. Hardacre, X. Fan, J. Huang, X. Tu, Shielding protection by mesoporous catalysts for improving plasma-catalytic ambient ammonia synthesis, Journal of the American Chemical Society, (2022).

[51] B.S. Patil, N. Cherkasov, N.V. Srinath, J. Lang, A.O. Ibhadon, Q. Wang, V. Hessel, The role of heterogeneous catalysts in the plasma-catalytic ammonia synthesis, Catalysis Today, 362 (2021) 2-10.

[52] P. Mehta, P. Barboun, F.A. Herrera, J. Kim, P. Rumbach, D.B. Go, J.C. Hicks, W.F. Schneider, Overcoming ammonia synthesis scaling relations with plasma-enabled catalysis, Nature Catalysis, 1 (2018) 269-275.

[53] K.H.R. Rouwenhorst, Y. Engelmann, K. van ‘t Veer, R.S. Postma, A. Bogaerts, L. Lefferts, Plasma-driven catalysis: green ammonia synthesis with intermittent electricity, Green Chemistry, 22 (2020) 6258-6287.

[54] S.L. Foster, S.I.P. Bakovic, R.D. Duda, S. Maheshwari, R.D. Milton, S.D. Minteer, M.J. Janik, J.N. Renner, L.F. Greenlee, Catalysts for nitrogen reduction to ammonia, Nature Catalysis, 1 (2018) 490-500.

[55] A.J. Medford, A. Vojvodic, J.S. Hummelshøj, J. Voss, F. Abild-Pedersen, F. Studt, T. Bligaard, A. Nilsson, J.K. Nørskov, From the Sabatier principle to a predictive theory of transition-metal heterogeneous catalysis, Journal of Catalysis, 328 (2015) 36-42.

[56] T. Wang, F. Abild-Pedersen, Achieving industrial ammonia synthesis rates at near-ambient conditions through modified scaling relations on a confined dual site, Proceedings of the National Academy of Sciences, 118 (2021) e2106527118.

[57] K.H.R. Rouwenhorst, H.-H. Kim, L. Lefferts, Vibrationally excited activation of N_2 in plasma-enhanced catalytic ammonia synthesis: A kinetic analysis, ACS Sustainable Chemistry & Engineering, 7 (2019) 17515-17522.

[58] V. Palma, M. Cortese, S. Renda, C. Ruocco, M. Martino, E. Meloni, A review about the recent advances in selected nonthermal plasma assisted solid–gas phase chemical processes, Nanomaterials, 10 (2020) 1596.

[59] K.A. Moltved, K.P. Kepp, The chemical bond between transition metals and oxygen: electronegativity, d-orbital effects, and oxophilicity as descriptors of metal–oxygen interactions, The Journal of Physical Chemistry C, 123 (2019) 18432-18444.

[60] L. Hollevoet, E. Vervloessem, Y. Gorbanev, A. Nikiforov, N. De Geyter, A. Bogaerts, J.A. Martens, Energy-efficient small-scale ammonia synthesis process with plasma-enabled nitrogen oxidation and catalytic reduction of adsorbed NO_x, ChemSusChem, 15 (2022) e202102526.

[61] J. Shah, W. Wang, A. Bogaerts, M.L. Carreon, Ammonia synthesis by radio frequency plasma catalysis: Revealing the underlying mechanisms, ACS Applied Energy Materials, 1 (2018) 4824-4839.

[62] P. Navascués, J.M. Obrero-Pérez, J. Cotrino, A.R. González-Elipe, A. Gómez-Ramírez, Unraveling discharge and surface mechanisms in plasma-assisted ammonia reactions, ACS Sustainable Chemistry & Engineering, 8 (2020) 14855-14866.

[63] Y. Gorbanev, E. Vervloessem, A. Nikiforov, A. Bogaerts, Nitrogen fixation with water vapor by nonequilibrium plasma: Toward sustainable ammonia production, ACS Sustainable Chemistry & Engineering, 8 (2020) 2996-3004.

[64] F.Y. Hansen, N.E. Henriksen, G.D. Billing, A. Guldberg, Catalytic synthesis of ammonia using vibrationally excited nitrogen molecules: theoretical calculation of equilibrium and rate constants, Surface science, 264 (1992) 225-234.

[65] T.-W. Liu, F. Gorky, M.L. Carreon, D.A. Gómez-Gualdrón, Energetics of reaction pathways enabled by N and H radicals during catalytic, plasma-assisted NH_3 synthesis, ACS Sustainable Chemistry & Engineering, (2022).

[66] Y. Engelmann, K. van 't Veer, Y. Gorbanev, E.C. Neyts, W.F. Schneider, A. Bogaerts, Plasma catalysis for ammonia synthesis: A microkinetic modeling study on the contributions of Eley–Rideal reactions, ACS Sustainable Chemistry & Engineering, 9 (2021) 13151-13163.

[67] J. Hong, S. Pancheshnyi, E. Tam, J.J. Lowke, S. Prawer, A.B. Murphy, Kinetic modelling of NH_3 production in N_2–H_2 non-equilibrium atmospheric-pressure plasma catalysis, Journal of Physics D: Applied Physics, 50 (2017) 154005.

[68] D. Xie, Y. Sun, T. Zhu, X. Fan, X. Hong, W. Yang, Ammonia synthesis and by-product formation from H_2O, H_2 and N_2 by dielectric barrier discharge combined with an Ru/Al_2O_3 catalyst, RSC Advances, 6 (2016) 105338-105346.

[69] T. Haruyama, T. Namise, N. Shimoshimizu, S. Uemura, Y. Takatsuji, M. Hino, R. Yamasaki, T. Kamachi, M. Kohno, Non-catalyzed one-step synthesis of ammonia from atmospheric air and water, Green Chemistry, 18 (2016) 4536-4541.

[70] D. Zhou, R. Zhou, R. Zhou, B. Liu, T. Zhang, Y. Xian, P.J. Cullen, X. Lu, K. Ostrikov, Sustainable ammonia production by non-thermal plasmas: Status, mechanisms, and opportunities, Chemical Engineering Journal, 421 (2021) 129544.

[71] C. Verheyen, T. Silva, V. Guerra, A. Bogaerts, The effect of H_2O on the vibrational populations of CO_2 in a CO_2/H_2O microwave plasma: a kinetic modelling investigation, Plasma Sources Science and Technology, 29 (2020) 095009.

[72] Y. Gorbanev, D. O'Connell, V. Chechik, Non-thermal plasma in contact with water: The origin of species, Chemistry – A European Journal, 22 (2016) 3496-3505.

[73] M. Kitano, J. Kujirai, K. Ogasawara, S. Matsuishi, T. Tada, H. Abe, Y. Niwa, H. Hosono, Low-temperature synthesis of perovskite oxynitride-hydrides as ammonia synthesis catalysts, Journal of the American Chemical Society, 141 (2019) 20344-20353.

[74] C. Foo, J. Fellowes, H. Fang, A. Large, S. Wu, G. Held, E. Raine, P.-L. Ho, C. Tang, S.C.E. Tsang, Importance of hydrogen migration in catalytic ammonia synthesis over yttrium-doped barium zirconate-supported ruthenium nanoparticles: visualization of proton trap sites, The Journal of Physical Chemistry C, 125 (2021) 23058-23070.